Nanoscale

Accepted Manuscript

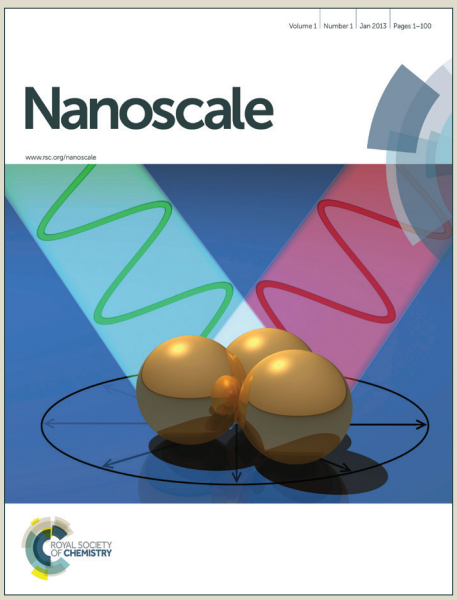

ROYAL SOCIETY OF CHEMISTRY

www.rsc.org/nanoscale

Nanoscale

RSCPublishing

COMMUNICATION

2D XANES-XEOL Mapping: Observation of Enhanced Band Gap Emission from ZnO Nanowire Arrays

Cite this: DOI: 10.1039/x0xx00000x

Zhiqiang Wang, Xiaoxuan Guo and Tsun-Kong Sham*

Received 00th January 2012,
Accepted 00th January 2012

DOI: 10.1039/x0xx00000x

www.rsc.org/

Using 2D XANES-XEOL spectroscopy, it is found that the band gap emission of ZnO nanowire arrays is substantially enhanced i.e. that the intensity ratio between the band gap and defect emissions increases by more than an order of magnitude when the excitation energy is scanned across O K-edge. Possible mechanisms are discussed.

In the past two decades, one-dimensional (1D) nanostructures have attracted extensive attention due to their unique and fascinating properties as well as their potential technological applications.[1-5] Among these, ZnO nanostructures have been widely investigated for a range of applications including flat panel displays, sensors, lasers, photovoltaic devices and energy harvesting.[6-12] With a direct band gap of 3.37 eV and a large exciton binding energy of 60 meV, ZnO nanowires (NWs) have been recognized as one of the most promising materials for the next generation optoelectronic devices operating in ultraviolet (UV) region, such as light-emitting diodes (LEDs), photodetectors, and solar cells.[11, 13-14] However, due to the high surface area to volume ratio of nanostructures, surface states play an important role on the optical properties of ZnO NWs; furthermore, the morphology, size, crystallinity and defect distribution all play significant roles in determining the luminescence.[15-16] Generally speaking, room temperature emission from ZnO NWs often exhibits a weak near band gap emission (BGE) in the UV region and a broad defect emission (DE) in the green region,[17-18] and sometime a broad surface defect peak in the red region,[16] although nearly perfect crystalline nanoneedles and well capped (surface states quenched), nearly perfect quantum dots exhibit dominantly the near BGE with little defect luminescence in the green band.[19-20] The unsatisfactory luminescence efficiency due to energy transfer to defect states prevents high device performance. To suppress the DE while enhancing the BGE of ZnO NWs, post-annealing treatment and surface modifications (e.g.: plasma immersion ion implantation (PIII), low energy argon ion milling, surface plasmon, surface passivation, and polymer covering) have been demonstrated with some success.[18, 21-24]

Recently, a new synchrotron-based spectroscopy technique, namely, two-dimensional X-ray absorption near-edge structure-X-ray excited optical luminescence (2D XANES-XEOL) spectroscopy, has been applied to study the nature of the optical luminescence from GaN-ZnO solid-solution nanostructures.[25] X-ray absorption near-edge structure (XANES) probes the local structure and bonding of the absorbing atom by monitoring the absorption coefficient above the absorption edge using tunable X-ray from a synchrotron light source. XANES can provide information on oxidation state, coordination, and symmetry of the system.[26] XEOL is a de-excitation spectroscopy which measures the optical response of the system upon excitation using photon with selected energy, often across an absorption edge of a given element of interest, providing elemental and in some cases, site specificity.[27,28] XEOL can also be used to track the XANES using the photoluminescence yield (PLY). A XANES spectrum recorded in PLY is equivalent to the excitation spectrum in the UV-visible region. XANES and XEOL can thus be used to reveal the element or the site that is responsible for the luminescence. When these two techniques are combined into 2D XANES-XEOL (or XAFS-XEOL) spectroscopy, one has the ability to extract the PLY at any optical wavelength as a function of incident X-ray energy, producing wavelength-selected optical-XANES spectra. Meanwhile, one can also extract excitation-energy-selected XEOL spectra, which enables the same elemental specificity gained from XANES to be applied to the optical luminescence response of a given material. More details about 2D XANES-XEOL spectroscopy can be found elsewhere.[25]

In this work, we report a 2D XANES-XEOL study of the optical luminescence from ZnO NW arrays excited by X-rays tuned across the O K-edge and the Zn $L_{3,2}$-edge. It is found that the XEOL spectra exhibit both near band gap and defect (green) emissions, which are very sensitive to excitations at both O K-edge and Zn $L_{3,2}$-edge. It is observed for the first time that the BGE from ZnO NW arrays is substantially enhanced i.e. that the intensity ratio between BGE and DE increases by more than an order of magnitude when the excitation energy is scanned across O K-edge. Two mechanisms at

interplay (thermalization of electrons and holes in the XEOL process and incident beam-induced annealing) are proposed for the improvement of crystallinity of ZnO NW (near surface region) that results in the enhancement of BGE in ZnO NW arrays.

The ZnO NW arrays used herein were synthesized on a silicon substrate via chemical vapor deposition as reported previously.[29] A Philips-XL30 scanning electron microscopy (SEM) and a Philips Tecnai F20 transmission electron microscopy (TEM) were used to characterize the morphology of the sample. Synchrotron measurements were carried out at the high resolution spherical grating monochromator (SGM) beamline at the Canadian Light Source (CLS)[30] The sample was mounted on a carbon tape with an angle of incidence of 45°. XANES were recorded in total electron yield (TEY), X-ray fluorescence yield (FLY) and photoluminescence yield (PLY). TEY and FLY were detected with the specimen current and the X-ray fluorescence photons respectively, and PLY was measured by detecting the optical photons emitted from the sample when the incident photon energies were tuned across an absorption edge of the element of interest (from a few eV below the edge to about 50 eV above the edge). Simultaneously, XEOL (~200-1000 nm) spectra were collected for the XANES scan at each and every step across the absorption edge using a dispersive optical spectrometer (QE65000, Ocean Optics). Thus, a 2D XANES–XEOL map can be created in which the vertical axis is the excitation energy and the horizontal axis is the luminescence wavelength and the luminescence intensity as a function of excitation energy and emission wavelength is color-coded. It typically took about 15 minutes to generate a 2D XANES–XEOL map at O K-edge or Zn $L_{3,2}$-edge reported here. The incident photon flux at the O K-edge and the Zn $L_{3,2}$-edge are about 5.5E12 and 1E12 photons/s/100mA, respectively. All XANES and XEOL spectra extracted from the 2D XANES-XEOL map were normalized to the incident photon flux collected on a refreshed Au grid. More details about synchrotron measurements can be found elsewhere.[25, 31]

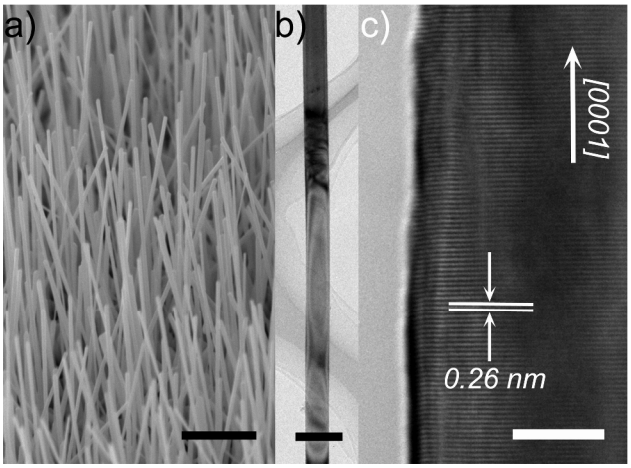

Figure 1. SEM, TEM and HRTEM images of the ZnO NWs. Scale bars in a), b) and c) are 2 μm, 200 nm and 5 nm, respectively.

The ZnO NWs were grown vertically on the Si substrate with a diameter in the range of 90-200 nm and a length of several micrometers as shown by the representative SEM and TEM images in Figure 1a and 1b, respectively. High-resolution TEM image (Figure 1c) shows clear lattice fringes of the (0002) plane of wurtzite ZnO with good crystallinity. The growth direction of the ZnO NWs is determined to be [0001].

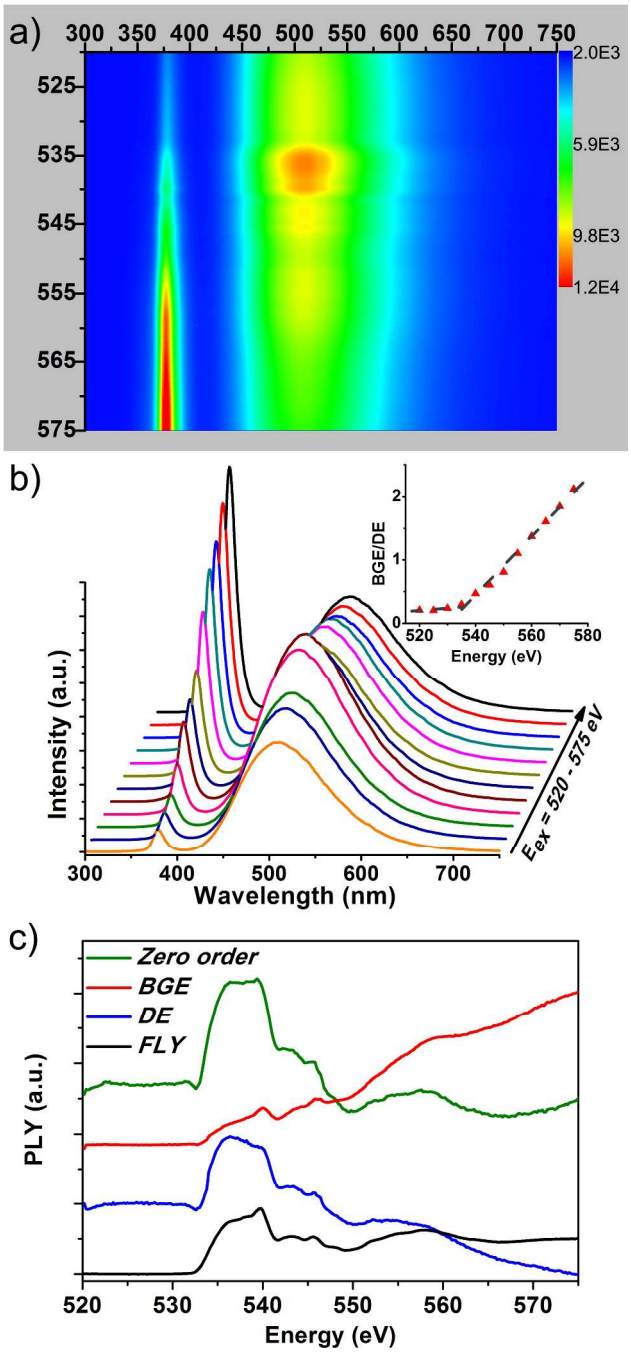

Figure 2. a) 2D XANES-XEOL map of the ZnO NW arrays with excitations at the O K-edge. The x-axis is the emission wavelength in nm and the y-axis is the excitation energy in eV. The color represents the intensity of XEOL excited across the absorption edge. b) XEOL cuts taken across the O K-edge (horizontal cuts taken in the 2D XANES-XEOL map). The inset shows the intensity ratio of BGE/DE (height) versus excitation energy. c) Wavelength-selected PLY (vertical cuts taken in the 2D XANES-XEOL map). FLY and zero order PLY are also shown for comparison.

Figure 2a displays the 2D XANES-XEOL map of the as-prepared ZnO NW arrays, in which the color represents the intensity of the XEOL excited across the O K-edge. Representative XEOL spectra at different excitation energies (horizontal cuts) and wavelength-selected PLY (vertical cuts) are shown in Figure 2b and c,

respectively. At first glance, the XEOL spectra of the ZnO NW arrays show one UV peak at 378 nm and one broad green peak at 509 nm, attributed to the BGE and DE (oxygen vacancies in the near surface region, evidence can be found in the Supporting Information) of ZnO, respectively. It is interesting to note that the XEOL spectra are very sensitive when tuning the excitation energies across the O K-edge, e.g., the BGE of the ZnO NW arrays is substantially enhanced while the DE is first increased (E_{ex} = 520-540 eV) and then decreased (E_{ex} = 540-575 eV).

Let us look at the 2D XANES-XEOL map in more detail. First, the DE is dominant in the XEOL spectra when the X-ray energies are below the threshold energy of the O K-edge (about 534 eV). The intensities of both the BGE and DE increase slightly when the X-ray energies are approaching the threshold. The intensity ratio (I_{BGE}/I_{DE}) measured by height remains approximately constant as shown in the inset of Figure 2b. Second, the intensities of both the BGE and DE increase markedly once the photon energies are just above the threshold energy (e.g., E_{ex} = 535 eV) while the intensity ratio changes a little. Third, the BGE of the ZnO NW arrays is significantly enhanced while the DE is decreased when the photon energy increases further (e.g., E_{ex} = 540-575 eV). The intensity ratio between the BGE and DE is substantially increased and a linear relationship exists between the intensity ratio and excitation energies (see the inset of Figure 2b). Comparing the XEOL spectra with excitation energy below and above the O K-edge, the intensity ratio I_{BGE}/I_{DE} increases by more than an order of magnitude. As shown in Figure 2c, the zero order PLY of the ZnO NW arrays is similar to their FLY XANES except for the height of the post-edge lines. But, striking differences are seen between the partial PLY recorded in the BGE and DE regions. 1) The PLY_{DE} exhibits a significant reduction in the feature at 539.7 eV that comes from excitation of an O 1*s* electron to $2p_{x+y}$ orbitals.[19] The $2p_{x+y}$ orbitals are directed radially toward the surface of the ZnO NW. The DE has been assigned to oxygen vacancies in the near surface region of ZnO nanostructures.[32] It indicates that the excited state reached following O 1*s* to $2p_{x+y}$ excitation does not couple strongly with the oxygen defect, while the BGE yield, which represents bulk properties, is very similar to that of the FLY. 2) Both the PLY_{BGE} and PLY_{DE} show positive edge jump, however the PLY_{BGE} exhibits a gradual increase in intensity while the PLY_{DE} a gradual decrease when the excitation energies are above the threshold energy of O K-edge.

Let us now turn to the Zn $L_{3,2}$-edge. As shown in Figure 3a, a 2D XANES-XEOL map of the ZnO NW arrays with excitation energies scanning cross the Zn $L_{3,2}$-edge was generated at a fresh sample spot (spot #2). The same phenomenon that BGE/DE increases with photon energy was observed (see the inset of Figure 3b). It is interesting to point out that the intensity ratio I_{BGE}/I_{DE} shows slight increases in the range of 1020-1060 eV and then big increases in the range of 1060-1075 eV. Even increasing the photon energy to 1075 eV, BGE is still a little bit weaker than DE (I_{BGE}/I_{DE} is about 0.9). The enhancement of BGE of ZnO NW arrays is more effective at O K-edge than Zn $L_{3,2}$-edge. As shown in Figure 3c, the zero order PLY and wavelength-selected PLY (PLY_{BGE} and PLY_{DE}) are similar to the FLY XANES. The fact that the XEOL yield mimics that of the X-ray absorption coefficient indicates that the sites that produce the luminescence are not distinct from the overall structure of the ZnO NW. The O K-edge and Zn $L_{3,2}$-edge results are both reproducible (see Figure S3 and S4 in Supporting Information).

These interesting phenomena can be explained in terms of the thermalization of electrons and holes in the XEOL process that improves the crystallinity of ZnO in the shallow region (near surface

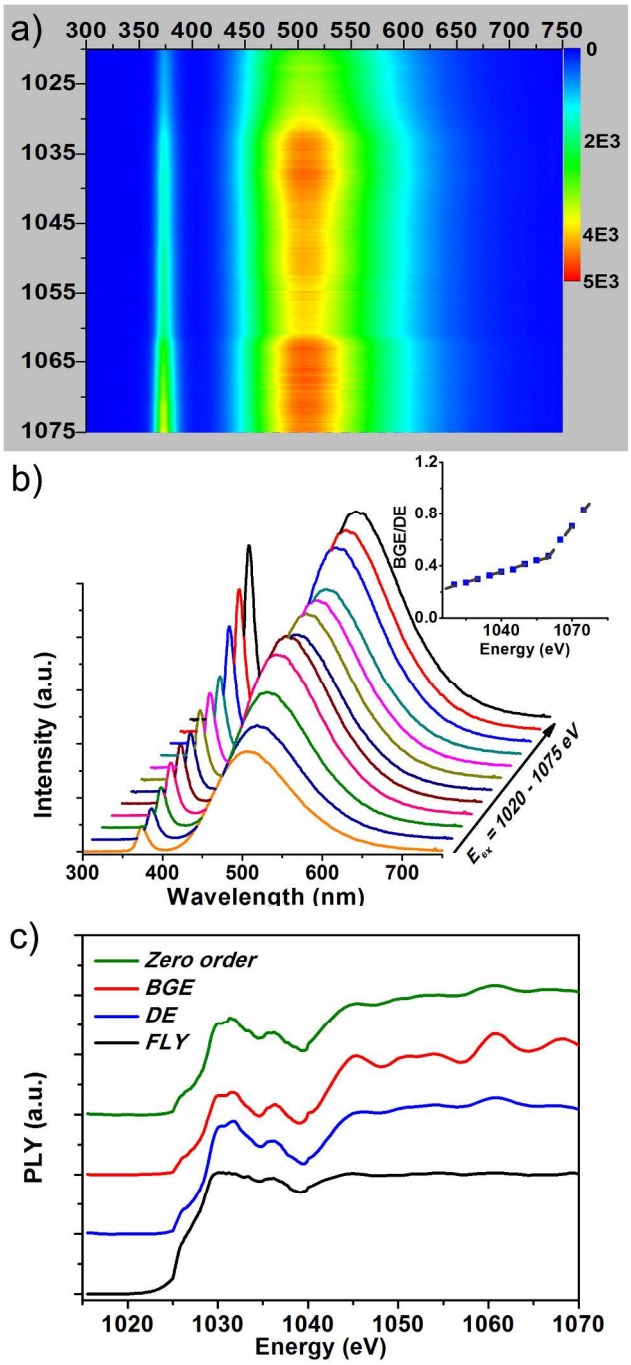

Figure 3. a) 2D XANES-XEOL map of the ZnO NW arrays with excitations at the Zn $L_{3,2}$-edge (obtained at a fresh spot). The color represents the intensity of XEOL excited across the absorption edge. b) XEOL cuts taken across the Zn $L_{3,2}$-edge (horizontal cuts taken in the 2D XANES-XEOL map). The inset shows the intensity ratio of BGE/DE versus excitation energy. c) Wavelength-selected PLY (vertical cuts taken in the 2D XANES-XEOL map). FLY and zero order PLY are also shown for comparison.

region) of the NWs. In the XEOL process, once an X-ray photon is absorbed at or just above the threshold, the core electron is excited to the conduction band. Then, Auger and fluorescence decay processes take place to fill the core hole, resulting in the creation of holes at outer shells and Auger electrons with excessive energy to excite

electrons at shallower levels (thermalization). Such secondary excitation continues and produces electron-hole pairs in a cascade manner until the energy is too low for further electronic excitation. The thermalization track is determined by the escape depth also known as the inelastic free mean path (IFMP) of electrons in solid (sometimes referred to as the universal curve with a minimum of a few Å at ~ 50 eV kinetic energy) and may be truncated by the dimension of the nanostructure. In semiconductors, the electron/hole undergoes thermalization until the electron reaches the bottom of the conduction band and the hole reaches the top of the valence band. Thermalization results in non-radiative (phonon) and radiative (optical) energy transfer. In the optical channel, electron and hole can form an electron-hole pair (exciton) that recombines and the energy is released either radiatively (optical photon) or non-radiatively (phonon). Energy transfer to defect states in the band gap can also take place, which in turn can also lead to luminescence in longer wavelengths and a decrease in the BG luminescence, since the two are competing. DE is absent in perfect crystallites.[15-16] Non-radiative energy transfer can result in radiation induced local annealing.

For the ZnO NW arrays, if the excitation energy is below the O K-edge, only electrons in the outer shell are excited into the upper bands then the continuum (similar to Cathodoluminescence but the electrons are of much lower energy and come from within).[33-34] XEOL of the ZnO NW arrays shows weak BGE and strong DE (see Figure 2a and b), which are commonly observed in ZnO nanostructures synthesized in oxygen-deficient environments.[29] The I_{BGE}/I_{DE} ratio changes little below the absorption edge (see the inset of Figure 2b). Once the photon energy is tuned above the threshold energy of the O K-edge, O 1s electrons are starting to be excited to the conduction band of mainly O character. In the secondary processes as mentioned above, the electron/hole undergoes thermalization until the electron reaches the bottom of the conduction band and the hole reaches the top of the valence band. Meanwhile, part of the excess energy transferring (non-radiative) contributes to the improvement of crystallinity of ZnO NWs (annealing via phonon electron coupling that decreases the amount of defects) in the shallow region of the nanostructures. Therefore, the BGE intensity increases at the expense of DE (perfect crystal only exhibits BGE). With further increase in photon energy, more excess energies are converted to improve the crystallinity of the ZnO NWs. As a result, the BGE keeps increasing with the excitation energy while the DE decreasing (see Figure 2a and b). The intensity ratio I_{BGE}/I_{DE} rises linearly with excitation energy (see the inset of Figure 2b).

At the Zn $L_{3,2}$-edge, however, the photon penetrates deeper and Zn 2p electrons are selectively excited to the conduction band. In this case, the thermalization of electrons and holes also contributes to the improvement of the crystallinity of the ZnO NWs as that at O K-edge. Therefore, similar phenomenon was observed when turning the photon energy across the Zn $L_{3,2}$-edge. Notice that the enhancement of BGE is more pronounced at O K-edge than Zn $L_{3,2}$-edge, although the X-ray attenuation length of both O K-edge and Zn $L_{3,2}$-edge is larger than the diameter of ZnO NWs. It can be due to the fact that the photon flux of O K-edge is about 5 times higher than Zn $L_{3,2}$-edge so that at O K-edge more excess energies contribute to reduce defect density. It leads to that such phenomenon is more obvious at O K-edge.

The second possible mechanism is that a chemical reaction occurred in the surface of ZnO NWs as a result of X-ray exposure. During the measurement, the chamber pressure is typically between 1E-7 and 1E-8 Torr that is lower than ultra-high vacuum (UHV). When ZnO NW arrays were illuminated by X-ray photon, the incident beam-induced sample heating can result in the reaction between the ZnO surface and the residual gas (mainly water). Since total electron yield (TEY) mode is surface sensitive, it can give information of the near surface region of ZnO NWs after X-ray exposure. TEY spectra in the first and second O K-edge scan (at spot #1) are shown in Figure S5 (see Supporting Information). After exposed to X-ray for about 25 min, the feature at 536.3 eV corresponding to O 1s to $2p_z$ transition becomes stronger in the red curve (the second TEY spectrum) that looks more similar to the FLY spectrum (black curve in Figure 2c). The same results were also found at Zn $L_{3,2}$-edge TEY spectra (see Figure S6 in Supporting Information). It indicates that the surface of ZnO NWs shows more bulk feature after X-ray exposure (defect density in the surface of ZnO NWs decreases). Clearly, X-ray exposure time can affect the luminescence of ZnO NWs. Time dependent XEOL spectra of the ZnO NW arrays were obtained from a new sample spot (spot #3) at 540 eV (see Figure 4). The black curve was measured once the ZnO NWs were exposed to the incident X-ray. It shows weak BGE and strong DE that is similar to those with excitation energy of 520-535 eV (the bottom four curves in Figure 2b). With the increase of exposure time, the BGE increases dramatically and the DE decreases (e.g.: at 5 and 10 min). The BGE becomes dominant when further increasing the time to 15 and 20 min (green and pink curve in Figure 4). After that, the luminescence of the ZnO NWs is stable indicating that the crystallinity of the ZnO NWs reaches a steady state.

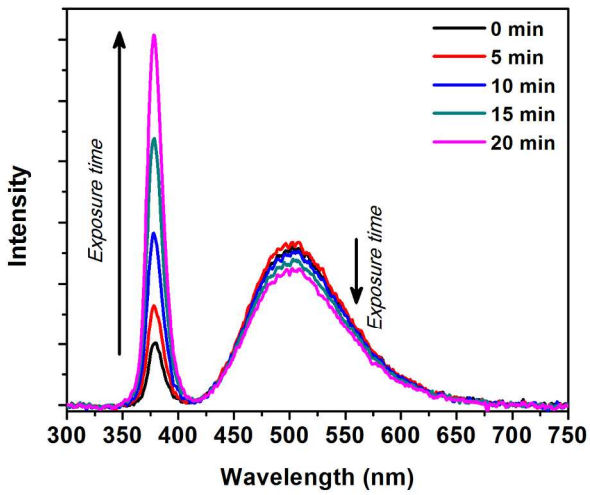

Figure 4. Time dependent XEOL spectra of the ZnO NW arrays at the O K-edge (E_{ex} = 540 eV). The XEOL spectra were collected when the ZnO NWs were irritated for 0, 5, 10, 15 and 20 min, respectively.

The enhanced BGE observed in the 2D XANES-XEOL maps at O K-edge and Zn $L_{3,2}$-edge (Figure 2 and 3) depends on both the thermalization of electrons and holes in the XEOL process and X-ray exposure time, but the first one plays more important role. Take the O K-edge as an example: i) in the time-dependent XEOL spectra (Figure 4), the intensity ratio I_{BGE}/I_{DE} increases about 2.5 times after 10 min exposure; ii) in the 2D XANES-XEOL map (Figure 2a), however that increases about 7.5 times when increasing the excitation energy from 520 to 560 eV (about 10 min, the same exposure time). Therefore, it is proposed that the thermalization of electrons and holes in the XEOL process plays predominant role in the enhancement of the BGE from ZnO NW arrays.

Apart from beam radiation induced annealing,[35] thermal induced desorption of surface species, such as oxygen, water, hydroxyl group, and advantageous molecules, can also result in the enhancement of the BGE of ZnO nanostructures.[36-39] To test the effect of adsorbates from ambient, we performed the following experiment. After the ZnO NWs were exposed to X-ray for 20 min (E_{ex} = 540 eV at spot #3), the incident beam was switched off and air was introduced into the chamber for 20 min at a pressure of 1E-5 Torr (a 12000 Langmuir exposure). Then, nitrogen, oxygen or water adsorbed on the surface of ZnO NWs during the synthesis and storage would have been readsorbed with this high exposure. In this case, the BGE would be quenched again and DE would be dominant if adsorbates from the ambient play a big role. However, the XEOL spectrum with 12000 Langmuir exposure (red curve in Figure S7 measured at spot #3) changes little compared to that with exposure time of 20 min to incident light (black curve). It indicates that thermal induced desorption of surface adsorbate has little effect on the behavior observed in Figure 2 and 3. Another possibility though less likely, is that synchrotron radiation induced desorption of oxygen (O^+) on the ZnO surface could result in a partially metallized surface (this effect has low cross-section.[40]). The localized coupling of surface plasmons of the metal (Zn) clusters could lead to the enhancement of BGE of ZnO nanostructures.[41-43]

Raman spectroscopy provides not only basic phase identification but also nano-scale structural changes. Raman spectra of the ZnO NWs with different I_{BGE}/I_{DE} ratios (I_{BGE}/I_{DE}: ZnO NWs < ZnO NWs-1 < ZnO NWs-2. ZnO NWs-1 and ZnO NWs-2 were prepared by the same method used for the synthesis of the ZnO NWs shown above, but the experiment parameters were different) are shown in Figure S8. E_2 (high) mode at 434.8 cm^{-1} that is associated with oxygen atoms is observed in all three ZnO samples. Noted that as shown in Figure S8b the intensity of E_2 (high) mode increases with I_{BGE}/I_{DE} ratio (related to the crystallinity of ZnO). Therefore, *In situ* Raman spectroscopy that monitors the E_2 (high) mode as a function of excitation energy and X-ray exposure time will help probe the changes happened at the near surface region of ZnO NWs in continuous XEOL processes, and provide better understanding of possible mechanism.

Conclusions

In summary, we have reported 2D XANES-XEOL map of the ZnO NW arrays across the O K-edge and Zn $L_{3,2}$-edge. We observe that the BGE in the ZnO NW arrays is significantly enhanced i.e. that the I_{BGE}/I_{DE} ratio increases by more than an order of magnitude when the excitation energy is scanned across O K-edge. The interplay of thermalization of electrons and holes in the XEOL process and incident beam-induced annealing is proposed for the improvement of crystallinity of ZnO NW surface that leads to the enhancement of BGE in ZnO NW arrays. We have also shown that the 2D XANES-XEOL technique provides a unique capability to investigate light emitting nanomaterials.

Acknowledgment. Research at the University of Western Ontario is supported by NSERC, CFI, OIT, OMRI and CRC (TKS). CLS is supported by CFI, NSERC, CHIR, NRC, and the University of Saskatchewan. Authors thank Dr. Yang Song and Ms. Fengping Xiao for their kind help in Raman measurement. Assistance from Tom Regier, the SGM beamline scientist at CLS is gratefully acknowledged.

Notes and references

Department of Chemistry, the University of Western Ontario. 1151 Richmond Street, London, Ontario N6A 5B7, Canada. Email: tsham@uwo.ca

Electronic Supplementary Information (ESI) available: XEOL spectra with different excitation energies. X-ray attenuation length vs. photon energy. Details of surface defect in ZnO NWs. The second O K-edge and Zn L-edge 2D XANES-XEOL maps. Comparison of the first and second TEY at O K-edge and Zn L-edge scans, respectively. Raman spectra of the ZnO NWs with different I_{BGE}/I_{DE} ratios. See DOI: 10.1039/c000000x/

1 A. P. Alivisatos, *J. Phys. Chem.-Us* **1996,** *100*, 13226.

2 Y. N. Xia, P. D. Yang, Y. G. Sun, Y. Y. Wu, B. Mayers, B. Gates, Y. D. Yin, F. Kim, Y. Q. Yan, *Adv. Mater.* **2003,** *15*, 353.

3 Z. L. Wang, *Adv. Mater.* **2003,** *15*, 432.

4 Z. R. Dai, Z. W. Pan, Z. L. Wang, *Adv. Funct. Mater.* **2003,** *13*, 9.

5 X. F. Duan, Y. Huang, Y. Cui, J. F. Wang, C. M. Lieber, *Nature* **2001,** *409*, 66.

6 C. J. Lee, T. J. Lee, S. C. Lyu, Y. Zhang, H. Ruh, H. J. Lee, *Appl. Phys. Lett.* **2002,** *81*, 3648.

7 Z. L. Wang, *J. Phys.-Condens. Matter.* **2004,** *16*, R829.

8 M. H. Huang, S. Mao, H. Feick, H. Q. Yan, Y. Y. Wu, H. Kind, E. Weber, R. Russo, P. D. Yang, *Science* **2001,** *292*, 1897.

9 Z. Y. Fan, D. W. Wang, P. C. Chang, W. Y. Tseng, J. G. Lu, *Appl. Phys. Lett.* **2004,** *85*, 5923.

10 J. Goldberger, D. J. Sirbuly, M. Law, P. Yang, *J. Phys. Chem. B* **2005,** *109*, 9.

11 M. Law, L. E. Greene, J. C. Johnson, R. Saykally, P. D. Yang, *Nat. Mater.* **2005,** *4*, 455.

12 Z. L. Wang, J. H. Song, *Science* **2006,** *312*, 242.

13 J. H. Lim, C. K. Kang, K. K. Kim, I. K. Park, D. K. Hwang, S. J. Park, *Adv. Mater.* **2006,** *18*, 2720.

14 H. Kind, H. Q. Yan, B. Messer, M. Law, P. D. Yang, *Adv. Mater.* **2002,** *14*, 158.

15 X. H. Sun, S. Lam, T. K. Sham, F. Heigl, A. Jurgensen, N. B. Wong, *J. Phys. Chem. B* **2005,** *109*, 3120.

16 L. Armelao, F. Heigl, S. Brunet, R. Sammynaiken, T. Regier, R. I. R. Blyth, L. Zuin, R. Sankari, J. Vogt, T. K. Sham, *Chemphyschem* **2010,** *11*, 3625.

17 H. B. Zeng, G. T. Duan, Y. Li, S. K. Yang, X. X. Xu, W. P. Cai, *Adv. Funct. Mater.* **2010,** *20*, 561.

18 R. Chen, Q. L. Ye, T. C. He, V. D. Ta, Y. J. Ying, Y. Y. Tay, T. Wu, H. D. Sun, *Nano. Lett.* **2013,** *13*, 734.

19 R. A. Rosenberg, G. K. Shenoy, L. C. Tien, D. Norton, S. Pearton, X. H. Sun, T. K. Sham, *Appl. Phys. Lett.* **2006,** *89*, 093118.

20 B. K. Woo, W. Chen, A. G. Joly, R. Sammynaiken, *J. Phys. Chem. C* **2008,** *112*, 14292.

21 Y. Yang, B. K. Tay, X. W. Sun, J. Y. Sze, Z. J. Han, J. X. Wang, X. H. Zhang, Y. B. Li, S. Zhang, *Appl. Phys. Lett.* **2007,** *91*, 071921.

22 S. W. Hwang, D. H. Shin, C. O. Kim, S. H. Hong, M. C. Kim, J. Kim, K. Y. Lim, S. Kim, S. H. Choi, K. J. Ahn, G. Kim, S. H. Sim, B. H. Hong, *Phys. Rev. Lett.* **2010,** *105*, 127403.

23 C. C. Lin, H. P. Chen, H. C. Liao, S. Y. Chen, *Appl. Phys. Lett.* **2005,** *86*, 183103.

24 K. W. Liu, R. Chen, G. Z. Xing, T. Wu, H. D. Sun, *Appl. Phys. Lett*. **2010,** *96*, 23111.

25 M. J. Ward, W. Q. Han, T. K. Sham, *J. Phys. Chem. C* **2011,** *115*, 20507.

26 T. K. Sham. *Synchrotron Radiation: Earth, Environmental and Materials Sciences Applications*; Minerological Association of Canada, Saskatoon; 2002.

27 T. K. Sham, R. A. Rosenberg, *Chemphyschem* **2007,** *8*, 2557.

28 A. Rogalev, J. Goulon, *Chemical Applications of Synchrotron Radiation, Part II: X-Ray Applications*; World Scientific, Singapore; 2002.

29 Z. Q. Wang, J. F. Gong, Y. Su, Y. W. Jiang, S. G. Yang, *Cryst. Growth Des*. **2010,** *10*, 2455.

30 T. Regier, J. Krochak, T. K. Sham, Y. F. Hu, J. Thompson, R. I. R. Blyth, *Nucl. Instrum. Meth. A* **2007,** *582*, 93.

31 Z. Q. Wang, C. L. Li, L. J. Liu, T. K. Sham, *J. Chem. Phys.* **2013,** *138*, 084706.

32 A. Janotti, C. G. Van de Walle, *Appl. Phys. Lett.* **2005,** *87*, 122102.

33 O. Lobacheva, P. L. Corcoran, M. W. Murphy, J. Y. P. Ko, T. K. Sham, *Can. J. Chem.* **2012,** *90*, 298.

34 O. Lobacheva, M. W. Murphy, J. Y. P. Ko, T. K. Sham, *Can. J. Chem.* **2009,** *87*, 1255.

35 A. Karuppasamy, A. Subrahmanyam, *Mater. Lett.* **2007,** *61*, 1256.

36 R. G. Xie, T. Sekiguchi, T. Ishigaki, N. Ohashi, D. S. Li, D. R. Yang, B. D. Liu, Y. Bando, *Appl. Phys. Lett.* **2006,** *88*, 134103.

37 R. G. Xie, D. S. Li, D. R. Yang, T. Sekiguchi, M. H. Jiang, *Nanotechnology* **2006,** *17*, 2789.37 R. G. Xie, D. S. Li, D. R. Yang, T. Sekiguchi, M. H. Jiang, *Nanotechnology* **2006,** *17*, 2789.

38 A. N. Gruzintsev, W. T. Volkov, *Semiconductors* **2011,** *45*, 1420.

39 J. Lee, J. Chung, S. Lim, *Physica E* **2010,** *42*, 2143.

40 R. A. Rosenberg, S. P. Frigo. *Chemical Applications of Synchrotron Radiation. Part I Dynamics and VUV Spectroscopy*; World Scientific, Singapore; 2002.

41 K. C. Hui, C. W. Lai, H. C. Ong, *Thin Solid Films* **2005,** *483*, 222.

42 H. Y. Lin, C. L. Cheng, Y. Y. Chou, L. L. Huang, Y. F. Chen, *Opt. Express* **2006,** *14*, 2372.

43 B. J. Lawrie, R. F. Haglund Jr, R. Mu, *Opt. Express* **2009,** *17*, 2565.

